3D Printing and Rapid Replication of Advanced Numerically Generated Rough Surface Topographies in Numerous Polymers

Jack Perris, Charchit Kumar,* Yang Xu, Manlio Tassieri, Mehmet E. Kartal, Nikolaj Gadegaard, and Daniel M. Mulvihill*

An approach to rapidly produce high-quality polymer surface topographies from numerically generated surfaces is presented. The approach uses an advanced surface generation tool to flexibly design surfaces with user-defined topography characteristics over a large range of surface roughness. Roughness instances with root mean square roughness 25, 50, and 100 μm are studied. 3D printing is used to create a master surface and polymer casting and injection molding are employed to enable rapid replication in various polymers. The cross-correlation ratio (CCR) and a mean difference approach were used to assess replication quality. Injection molding provides high throughput with high replication quality up to CCR $\approx$ 0.74. While casting in low-viscosity polymer resins enables slightly improved high-quality replication (CCR up to $\approx$0.82) with reduced throughput. Key results include the ability of the 3D-printed surfaces to replicate tailored variations in surface topography (e.g., amplitude and frequency) and the importance of low viscosity resins in maximizing replication quality in polymer casting. Several interfacial and surface phenomena (both mechanical and biological) are sensitive to surface roughness. The main application lies in providing a valuable tool for research looking at topography influencing phenomena ranging from friction and lubrication to aerodynamic drag, algae growth, and cell growth.

J. Perris, C. Kumar, M. Tassieri, N. Gadegaard, D. M. Mulvihill
James Watt School of Engineering
University of Glasgow
Glasgow G12 8QQ, UK
E-mail: Charchit.Kumar@glasgow.ac.uk; Daniel.Mulvihill@glasgow.ac.uk

Y. Xu
School of Mechanical Engineering
Hefei University of Technology
Hefei 230009, China

M. E. Kartal
School of Engineering
University of Aberdeen
Aberdeen AB24 3UE, UK

The ORCID identification number(s) for the author(s) of this article can be found under https://doi.org/10.1002/adem.202200832.

1. Introduction

All surfaces exhibit what we call "roughness" on some scale. Indeed, the characteristics of surface roughness have an important bearing on several interfacial processes including friction, adhesion, and lubrication behavior to cell growth and algae growth. In general, the roughness we get on surfaces is a somewhat unpredictable byproduct of the manufacturing or formation process or indeed of wear and erosion processes. Such roughness is often multiscale containing randomness at various scales. This makes it difficult to control or design multiscale rough surfaces with predefined properties for use in either research or applications. To address this important shortfall, this article develops novel approaches to fabricate and rapidly replicate controlled and tailored rough polymer surfaces with advanced predefined topography characteristics.

The field concerned with designing surfaces is known as "surface engineering." Typically, the aim is to design and manufacture surfaces with properties that optimize functionality. Surface modifications are needed in various engineering applications including friction control, adhesion control, and aerodynamic drag reduction. A wide range of manufacturing methods are employed to engineer surfaces in a vast array of materials. These range from micro-injection molding, milling, laser structuring, embossing, treatments and coatings, additive manufacturing, various lithography process methods, surface replication, etc. For example, injection molding or 3D printing can be used to fabricate surfaces for microfluidic devices[1,2] or MEMS.[3,4] Laser structuring can be employed to improve surface performance in areas such as optical devices,[5] solar cell design,[6,7] metallic joints,[8] biomedical surfaces and implants.[9,10] Surface replication and molding are particularly prevalent in the field of biomimetics and are used to improve the replication and addition of bio-inspired design to modern engineering solutions.[11–15] However, the existing processes for generating controlled surfaces using these techniques are usually limited to structured surfaces (such as the squarewave in Refs. [1,16,17] rather than to complex, irregular, multiscale rough surfaces. In this work, we combine an advanced surface

generation approach with three fabrication techniques to produce a versatile novel tool for the rapid fabrication of pre-defined rough surfaces in numerous polymers. The three techniques we use are: 3D printing, micro-injection molding, and replication.

Typically, when 3D printing is used at the micro-scale, the designs are based on simple idealized geometrical arrangements—such as for optical devices,[18] microfluidic devices,[19–23] and micro-gears.[24] In the present work, however, the goal is to generate an irregular rough surface topography, but 3D printing is an ideal candidate as it can (within resolution limitations) follow an arbitrary surface topography. Thus, as the first step in the process, a stereolithography (SLA) 3D printing process was used to produce the designed rough surface topographies from numerically generated surfaces. The printed topographies could then be utilized for either polymer casting or modified for use as an injection molding inlay. The SLA process allows the resin to be cured using a laser to produce predefined patterns, building the designed components layer by layer. Irregular topography additive manufacture has generally been focused in areas of biomedical engineering related to tissue engineering or scaffolds for rehabilitation purposes.[25–28] The production of irregular micro-topographies in this study, on the other hand, is aimed at the rapid fabrication of near-exact copies of pre-generated rough surfaces with advanced control over surface topography characteristics. This is intended mostly for its use in research activities involving interfacial phenomenon sensitive to surface roughness (including, to mention but a few: friction, adhesion, contact stiffness, lubrication, fluid flow, etc.). The techniques developed in this work drew inspiration from the 3D printing of rough surfaces by Benett et al.[29] for the 2017 Contact Mechanics Challenge.[30] However, in Benett et al.,[29] the 3D-printed surface information was taken from a measured surface; whereas, the present work adds the powerful addition of an advanced and versatile approach/tool for controlled numerical rough surface generation prior to 3D printing. Another major development in the present article is the addition of two versatile surface replication routes (carried out after 3D printing) that enable rapid production in a wide range of polymers; namely injection molding and polymer replication.

Injection molding is a widely used polymer manufacturing method. Its uses can range from macroscale manufacture for products such as toys and furniture, to micro- and nano-scale manufacture.[20,31–34] It is often used in the polymer manufacturing industry due to its efficiency, accuracy, low fabrication costs, and high throughput. The process also allows many thermoplastic materials to be used, making it highly versatile.[34] The high accuracy has prompted researchers to explore its use in surface engineering to produce highly accurate replicas of micro and nanostructured topographies.[1,17] This makes the process ideally suited for the rough surface challenge being addressed in this work. However, there are many variables that can alter the performance of the injection molding process, and by extension, the quality of the components produced. Important molding parameters include injection velocity, holding time and pressure, mold temperature, polymer melt temperature, mold inlay design and material. All these parameters must be optimized to ensure the best output from the process and the greatest part fidelity.[30,35] The mold inlay fabrication and quality are particularly important in injection molding. The inlays or inserts can be fabricated in a

vast number of materials using a wide range of processes depending on the required component. Metals are typically the preferred material as they combine strength with high thermal conductivity. This results in durable tooling that can provide fast mold cycle times due to the metal's high thermal conductivity. Rapid cooling can have its drawbacks though as this can quickly freeze the molten polymer before the mold cavity has properly been filled; thereby, reducing part quality.[36] Metal inlays can be manufactured by micro electrical discharge machining, micro-mechanical milling, and electrochemical milling,[37–39] all of which are costly and introduce undesirable part roughness. A widely used alternative for inlay fabrication is Lithography, Electroplating, and Molding (LIGA). This process allows a replica of a topography to be made by electroplating the master surface which is then separated and used as a molding insert to make polymer replicas of the original substrate topography.[40] Here, we use a 3D-printed mold insert closely following the approach taken by our colleagues Convery et al.[33] who used 3D-printed mold inserts in the injection molding production of microfluidic components. 3D-printed inserts for injection molding have previously been used to fabricate micro-structured devices by other authors too.[21,22,41] Indeed, additive manufacturing is becoming an established process for injection molding inlay fabrication with wide scope for novel engineering applications.

The second route we deploy for rough surface replica production is the method of polymer casting. This technique is ubiquitous in the area of biomimetic surface replication, where complex topographies occurring in nature are duplicated and studied for scientific and engineering applications. The process works by pouring liquid polymer onto a surface (substrate/master) to generate a negative impression of the topography. This can be followed by a subsequent polymer casting step to generate a positive copy of the original substrate surface.[15,23,42,43] The replication method is often employed to emulate certain characteristics displayed by topographies. When engineered surfaces are designed there are generally certain characteristics specific to the systems design that will be desired and will influence how the surface interacts with its working environment. There will often be topographies in nature that display an optimum design that can provide the desired characteristics and these can be replicated in engineered surfaces by means of polymer casting. Some examples include emulating the hydrophobicity displayed by certain leaves,[44] anti-fouling mechanisms for marine and aerofoil systems,[45,46] light harvesting properties of plants[47] and self-cleaning and anti-reflective properties to improve solar cells.[48] The areas of application of polymer surface replication are thus extensive. This has resulted in a wide range of polymer materials being utilized to achieve optimized surface replication with desirable topography properties.[44,47,49,50] Therefore, this method is also a prime candidate for the replication of the 3D-printed designed topographies. Particularly, as it facilitates high-quality replication in a range of materials, allowing for versatility in the production of these complex polymer rough surface topographies.

The overall approach we take here may be summarized as follows. First, an advanced MATLAB code is used to generate predefined rough surface topographies. Then, the numerically generated surface is 3D-printed to produce a master surface.

**ADVANCED
SCIENCE NEWS**

www.advancedsciencenews.com

**ADVANCED
ENGINEERING
MATERIALS**

www.aem-journal.com

Finally, injection molding and casting are deployed as two alternative routes to rapid replication in a range of polymers. Details of the surface fabrication are given in Section 2. Methods are then required to check the fidelity of the replicated surfaces with the master and the numerically generated surfaces. Two approaches are used to achieve this: the cross-covariance method and a point-to-point mean difference measurement approach and these are outlined in Section 3. Finally, in Section 4, we analyze the effectiveness of the results. Most importantly, how well the 3D-printed master replicates the generated surface (Section 4.1) and how well the final rough surface replicas match the 3D-printed master (Section 4.2). We also study the mold inlay durability in injection molding (Section 4.3), the responsiveness of the process to reflect changes in topography—i.e., ability to tailor (Section 4.4) and the effect of resin viscosity on the effectiveness of replication using polymer casting. Finally, we discuss the many diverse applications of the new tool in Section 4.5 before making some final remarks.

2. Experimental Section

2.1. Surface Generation

Three topographies of distinct areal root mean squared surface roughness, Sq, were generated for study. The surfaces were generated to mimic the multiscale nature of real engineering rough surfaces. Many algorithms developed in previous literature can be used for this purpose.[51–54] This enabled the researchers to customize the roughness parameters and the spectral contents of the roughness topography. The rough surface $h(x,y)$ is generated based on an axisymmetric power spectrum density (PSD) $S(f_x, f_y) = S(f) = \sqrt{f_x^2 + f_y^2}$ defined in the frequency (inverse of the wavelength) domain as shown in **Figure 1**. The PSD value decreases in a power law behavior between the lower and upper cut-off frequencies f_l and f_s as

$$S(f) = C_0 f^{-2-2H} \quad f \in [f_r, f_s] \tag{1}$$

The PSD value elsewhere is strictly zero. $H \in [0,1]$ is the Hurst dimension.

The generated rough surface has lateral dimensions $L_x \times L_y$. Consider a periodic rough surface topography $h(x,y)$ with a period of L_x and L_y in the x- and y-directions, respectively. The following Fourier transform pair is used (Equation (2) and (3))
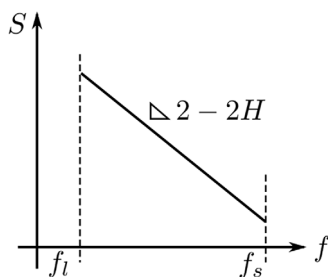
$$h(x,y) = \sum_{k=-\infty}^{\infty} \sum_{m=-\infty}^{\infty} H_{km} e^{+i2\pi\left(\frac{kx}{L_x}+\frac{my}{L_y}\right)} \tag{2}$$

$$H_{km} = \frac{1}{L_x L_y} \int_0^{L_x} \int_0^{L_y} h(x,y) e^{-i2\pi\left(\frac{kx}{L_x}+\frac{my}{L_y}\right)} dx dy \tag{3}$$

where $f_x = k/L_x$, and $f_y = m/L_y$. Since the auto-correlation function and the PSD also follows the above Fourier transform pair, we immediately have the following identity

$$S(f_x, f_y) = H_{km}\overline{H_{km}} = |H_{km}|^2 \tag{4}$$

Given that $S(f_x, f_y)$ is known from Equation (1), we can reconstruct the complex spectral H_{km} based on its absolute value $|H_{km}|$ solved by Equaiton (4) and a random phase $\theta_{km} \in [0, 2\pi)$

$$H_{km} = |H_{km}|[\cos(\theta) + i\sin(\theta)] \tag{5}$$

The random phase can result in non-repeatable realizations. Substituting H_{km} into the inverse Fourier transform in Equation (2) over a discretized frequency domain, produces the final generated topography. Equation (2) can be accelerated using the fast Fourier transform. An example of the generated topography is shown in **Figure 2**. The PSD of the generated rough topography has a good agreement with the target PSD given in Equation (1). The aforementioned approach was implemented via MATLAB. The rough surface topography with the desired parameters can then be used to produce an STL file suitable for use by 3D printers.

The roughness parameter used to primarily designate the generated and manufactured surfaces was the areal root mean square height of each surface, Sq. The generated surfaces were designed to have Sq values of 25, 50, and 100 µm. The rough surface areas produced measured 25 mm × 25 mm and integrated into a surrounding design depending on their fabrication procedure. For polymer casting, a border measuring 30 mm × 30 mm was included around the rough surface design. This indicates a distinct boundary between the rough topography edge and creates a cavity for the generated surface design allowing for simple casting. For injection molding, the three rough surface designs were integrated into a block design measuring 27.7 mm × 77.7 mm × 5 mm to fit the existing tooling of the injection molding machine.

2.2. 3D-Printed Rough Surface Master

The numerically generated surfaces were printed using a Form3 printer (FormLabs, USA) in the FormLabs proprietary Clear V4 resin.[55] The generated rough surface in STL file format was used as the input to the 3D printer. The Form3 printer uses an SLA process along with the photocurable resins. The SLA process allows the resin to be cured using a laser to produce predefined patterns, building the designed components layer by layer. This process was selected due to its high dimensional accuracy, fast fabrication times for the surfaces, and ease of use for users. The SLA printing process is well-established and used by many commercial printers that are readily available to future users of this process. The components are built directly onto a vertically
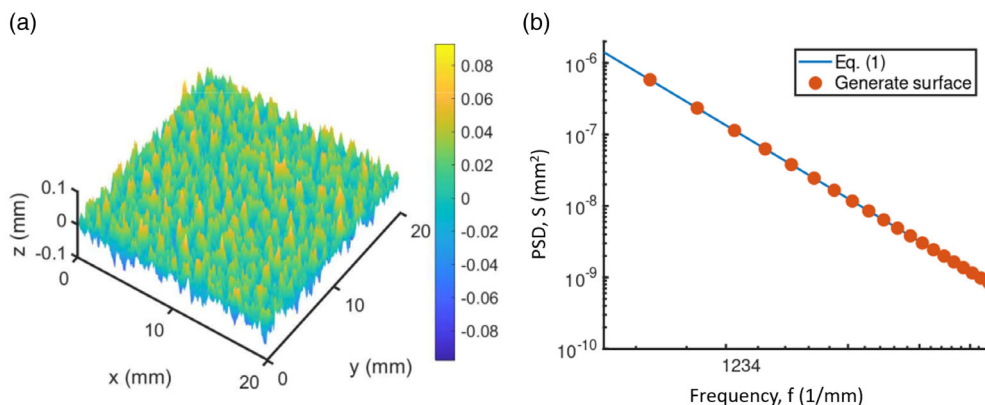

Figure 1. Schematic of the log–log plot of an axisymmetric power spectrum density (PSD).

Figure 2. a) Example 3D plot of the generated topography and b) Comparison between the radially averaged PSD $S(f) = \frac{1}{2\pi}\int_0^{2\pi} S(f,\theta)d\theta$ of the generated topography in (a) and the deterministic form in Equation (1). The lateral size is $L_x = L_y = 20$ mm; Parameters in the deterministic PSD are: $f_l = 10/L_x$, $f_s = 128/L_x$, $H = 0.7$, $C_0 = 1.7064 \times 10^{-5}$; $S_q = 25\,\mu m$. Number of sampling points: 256×256.

moving build plate, which rises out of the resin as layers are cured accordingly. Once the components are completed, they are removed carefully from the build plate and then transferred to a cleaning unit to remove any excess resin. The cleaning unit (Form Wash, FormLabs, USA) submerges the components in isopropyl alcohol while agitating them for a 10 min period. The partially cured or "green" components are then dried before being cured by UV light for 30 min at 60 °C (Form Cure, FormLabs, USA).

2.3. Replication from the Master Surface

Two replication methods were employed to manufacture replicas from the 3D-printed rough surface masters: injection molding and polymer casting. Both manufacturing methods offer high replication quality, but allow for individual additional benefits. Injection molding was considered as this allows high-quality replicas to be manufactured from the same inlay or master. This is particularly useful when rapid prototyping or for experimental production runs. The high throughput capabilities of injection molding allow for the rapid production of high-quality samples. The process allows for precise replication down to the nanoscale, depending on the tooling utilized.[28,29] However, the polymers available for injection molding are typically limited to thermoplastic materials. Therefore, polymer casting was selected for its ability to produce high-quality replicas from complex micro- and nano-structures and for its versatility in terms of available materials.[8–12] In general, the process is relatively simple. Its use is well documented in the biomedical engineering field for prototyping microfluidic devices by casting the elastomer polydimethylsiloxane (PDMS) onto an etched silicon master.[11] Various other types of polymers (polyvinyl siloxane (PVS), polypropylene (PP), polymethylmethacrylate (PMMA)) have also been cast onto natural surfaces to capture complex topographies for use in biomimetic research.[15,21–23,39–44]

2.3.1. Injection Molding

As mentioned, the 3D-printed topography was used as the tooling inlay for injection molding. A simplified process diagram is detailed in **Figure 3**. The key parameters to consider for injection molding include mold temperature, injection velocity, tooling temperature, holding pressure, and time. An optimization of these parameters is crucial to ensure comprehensive replication of complex micro-topographies from the rough surface 3D-printed inlays. For the present study, polystyrene (PS) (1810 Crystal Polystyrene, Total Petrochemical and Refining, Belgium) was selected due to its durability and high-quality replication capabilities. Injection molding was executed using a Victory 28 injection molding machine (Engel, Austria). The polymer was heated to 260 °C before being injected at a velocity of $1\,cm^3\,s^{-1}$ into a volume of $4\,cm^3$. The polymer was held in the mold cavity to cool for 35 s at a pressure of 800 bar. The cavity was then marginally opened to allow for further cooling. The relatively long molding cycle ensures polymer component fidelity and avoids distortion. The reduced thermal conductivity of a polymer insert results in longer cooler times than with typical metal mold inserts. Once adequate component cooling is achieved, the tool is opened and carefully ejected from the cavity. The process of integrating this 3D-printed material for use as an injection molding inlay was developed and optimized by Convery et al.[28]

2.3.2. Polymer Casting

The casting replication method adopted in this work uses the 3D-printed topography as the initial mold. The chosen polymer is then cast onto the 3D-printed topography and left to cure according to the manufacturer's instructions (which vary according to the polymer). Three different polymers were used to produce replicas using the casting method: ultra-low viscosity epoxy resin, PDMS, and polyvinyl siloxane (PVS). PVS used a slightly modified procedure and this is detailed in Section 2.3.3.

The procedure for Epoxy and PDMS is as follows. Initially, the 30 mm × 30 mm 3D-printed samples were glued down onto a plastic petri dish. The molding polymer mixture was then slowly poured onto the 3D-printed rough surface sample and allowed to cure. The polymer mixtures must be poured at a steady rate to avoid trapping air between the rough surface topography and the molding material. A simplified process flow is detailed in
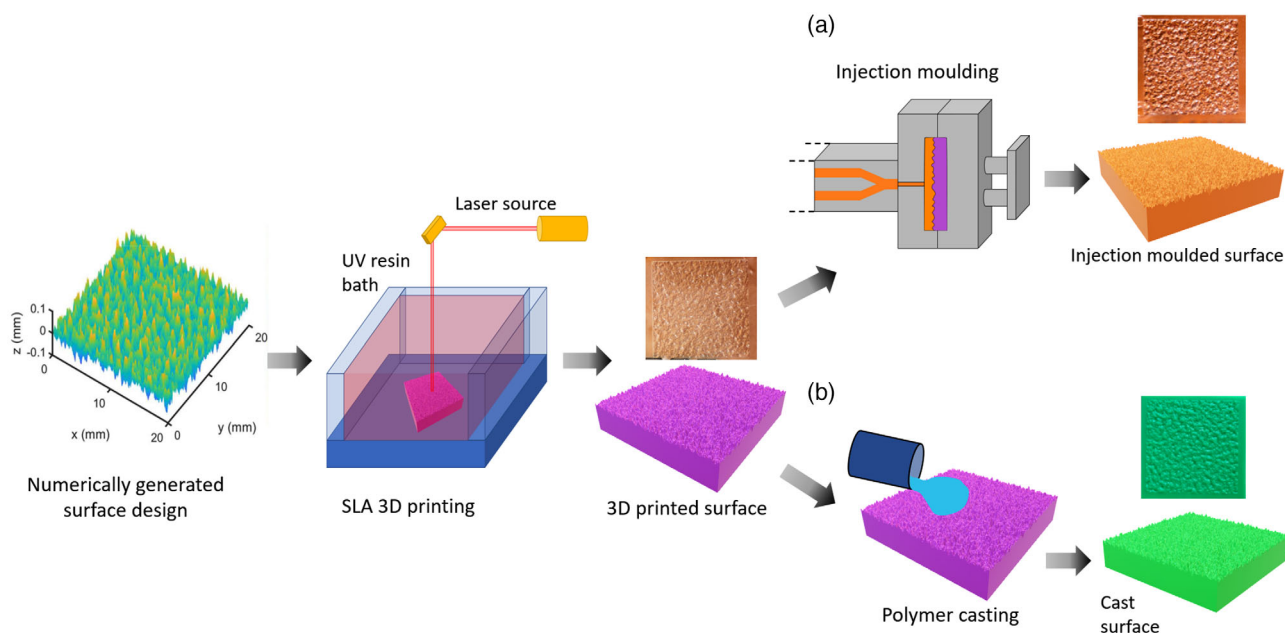
**ADVANCED
SCIENCE NEWS**

www.advancedsciencenews.com

**ADVANCED
ENGINEERING
MATERIALS**

www.aem-journal.com

Figure 3. Simplified process diagram detailing polymer fabrication routes utilized to produce rough surface topographies. a) Injection molding process flow, and b) polymer casting process flow.

Figure 3. Both polymers were mixed according to manufacturer instructions and then degassed in a vacuum chamber to remove any trapped dissolved air bubbles from the mixtures before casting. The epoxy resin (Epoxy Resin L & Hardener S, Conrad Electronic SE, Hirschau, Germany) consisted of two components that were mixed with a ratio of resin to hardener of 10:4.8 in a container for 5 min. The mixture was then degassed for 15 mins. Once poured onto the rough surface samples, the mixture was left to cure for 15 h at room temperature ($20 \pm 2\,°C$) as per manufacturer guidelines. The curing time can be reduced considerably: for example, to 10 h at 50 °C. This temperature can be further increased if faster processing times are required. Developed epoxy replicas were then carefully removed from the 3D prints. The PDMS follows a similar procedure: two-component PDMS (Sylgard 184 Silicone Elastomer, Dow Inc., USA) was uniformly mixed (monomer to crosslinker ratio 10:1) and degassed 3–4 times for 5 min periods to properly remove any trapped air bubbles. The clear mixture was then carefully poured over the 3D-printed samples to avoid trapping any air. The samples were then degassed again for 30 min to remove any excess trapped air at the interface between the PDMS mixture and the sample. The samples were finally cured in an oven for 4 h at 60 °C. The cured PDMS replicas were then carefully peeled from 3D-printed samples.

2.3.3. PVS Replica Molding

The PVS (President, Coltene Whaledent, Altstätten, Switzerland) replica molding method is similar to the polymer casting procedure (described in Section 2.3.2); however, the mixing of the monomer and curing agent is fixed by the manufacturer as the material is dispensed using an applicator gun. The dispenser

nozzle mixes the material at the same ratio for each replica PVS is typically used in dentistry to produce imprint molds capturing the complexity of a patient's teeth. This makes the material an ideal candidate for replicating complex rough surface topographies. The PVS mixture is applied slowly onto the 3D-printed samples to minimize trapped air at the substrate mold material interface. Once the sample area is covered, a flat PMMA plate is used to gently press the PVS into the 3D-printed sample. This ensures complete coverage and filling of the microcavities of the topography. The process is slightly modified from the procedure described in Figure 3. The pressing of the PVS is executed due to the increased viscosity and low flow rate of the PVS resins. The PVS polymerizes quickly and will fully cure after 10 min at room temperature. Once the PVS is cured, the replica is gently peeled from the 3D-printed mold sample. The ultra-light body PVS resin was used to create replicas of all three rough surface topographies (i.e., the three roughness Sq levels). A study on how the viscosity of the polymer mixture influences the replication quality was also conducted using PVS. To achieve this, four PVS products with increasing viscosity were used; namely, ultra-light, light, regular, and heavy body mixtures. The resins of varying viscosity were tested on the $Sq = 25\,\mu m$ topography for comparison. Additional photos of 3D-printed, injection molded, and cast surfaces are given in Figure S1 in Supporting Information.

2.4. Surface Characterization

The surface topography characterization of the 3D-printed masters and their polymer replicas were carried out using optical profilometry (InfiniteFocus, Bruker-Alicona, Austria). The 3D optical profilometer was used using the 5x optical zoom.

Critical measurements were taken at 12 distinct and set locations across each sample. These points were aligned and measured from set points to ensure consistency of measurement areas across the 3D print topographies and the polymer replicas. The metrology scans were collected and used to quantify the replication quality and assess the capabilities of the fabrication processes used. For injection molding, Parts 10, 20, and 30 in the molding cycle were analyzed. This allowed the assessment of replication quality across the different rough topographies on multiple parts. It also allowed for the assessment of inlay durability during the injection molding run. For the casting method, three replicas for each topography and material were created and then measured using the predefined scanning protocol. The scans over all samples were used for assessment of the quality of replication using two different methods discussed next.

3. Quantifying Replication Quality

Two methods were employed for analyzing the surface replication quality in both fabrication methods: the cross-covariance method and the "point-to-point difference measurement" method. The 12 individual scans on each sample were used to compare the 3D print to the polymer replicas. The parameters used allowed quantitative analysis of both line and surface profiles obtained from the optical scans of the surface.

3.1. Cross-Correlation Method

The primary analysis parameter we used to quantify the replication quality is the normalized cross-correlation ratio (CCR). This parameter allows quantification of the extent of the similarity between line profiles taken from the optical scans of the 3D prints and their replicas. The cross-correlation function is defined by the ratio of covariance to root-mean variance as

$$CCR = \frac{\sum_{i,j}\left[(Z_A(i,j) - \overline{Z}_A)(Z_B(i,j) - \overline{Z}_B)\right]}{\sqrt{\sum_{i,j}(Z_A(i,j) - \overline{Z}_A)^2}\sqrt{\sum_{i,j}(Z_B(i,j) - \overline{Z}_B)^2}} \quad (6)$$

where Z refers to the height of a profile at a point "i, j" in the plane. The subscript A typically refers to the original profile of the 3D-printed topography, while B refers to the profile of the polymer replica. $\overline{Z}$ represents the mean value of the height of the profile being considered. The value of the CCR can vary from 0 to 1: a value of unity indicates identical profiles (i.e., identical replication in this case) while a value close to zero indicates completely dissimilar and unrelated profiles (i.e., very poor replication). The average from nine profiles on the surfaces was used to generate CCR values. The function was suggested by the National Institute of Standards and Technology[56] and sees widespread use in assessing similarity between signals. For example, it was used by Kumar et al.[44] to analyze the replication quality between complex leaf topographies and their polymer replicas.

3.2. Point-to-Point Difference Measurement

The secondary method we used to quantify the quality of replication is based on a mean point-to-point difference between the two surfaces. This was implemented via the "Difference Measurement" module in Alicona's InfiniteFocus software (Bruker-Alicona, Austria). **Figure 4** shows a simplified process flow for the method. Scans of the same area are taken from predefined positions on the 3D prints and polymer replicas and these are then input to the difference module for comparison. The 3D-printed master surfaces were treated as the reference geometry and then compared to the respective polymer replica datasets. The individual datapoints in the scans are compared and measured to evaluate the disparity between the topography data. The module allows for automatic alignment but is restricted to datasets that have a minimum of 80% identicality.[57] Once automatically aligned, the dataset comparison can be measured. The difference in height measurement between the datasets
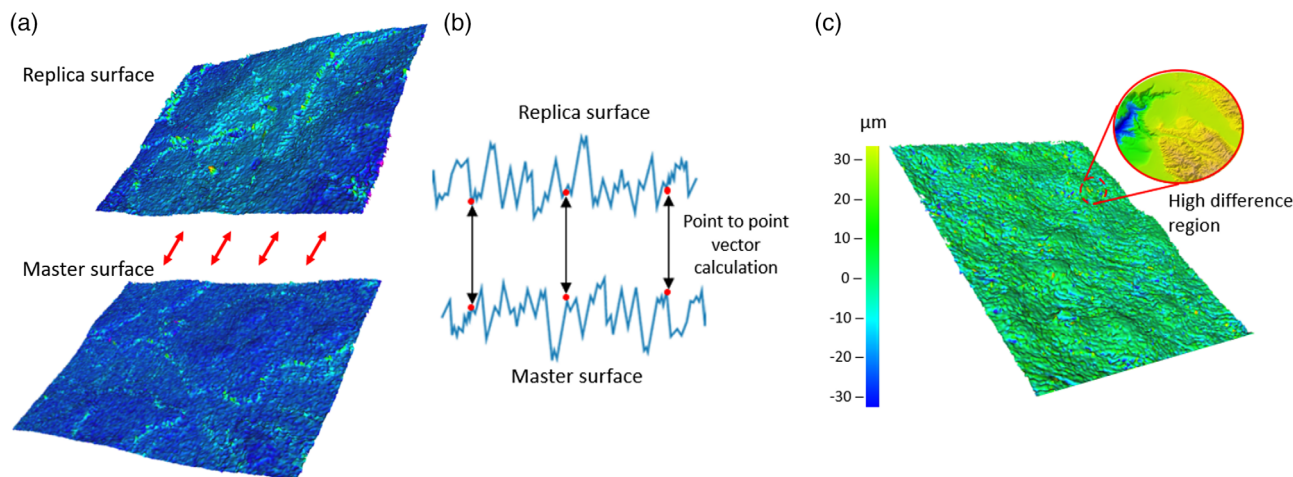

Figure 4. 3D mesh point-to-point surface comparison. a) Initial topography datasets are aligned based on similarity of the 3D mesh of surface point datasets, b) 2D representation of the direction vector generation and displacement calculation between data points in the topography datasets. c) heat map conveying the height difference between the surface datasets, this is an indication of the similarity of the surface datasets.

works by generating a 3D vector between the closest two respective data points and measuring the mean displacement vector between the data points. The automatic alignment facilitates a minimization of error in the comparison of incorrect data points. This comparison is then mapped across the surface dataset geometries to output a mean value for the difference in height between the topographies. Clearly, low values of mean difference indicate the best replication. The results from the difference measurement results are used as an alternative approach to verify trends in the CCR results.

4. Results and Discussion

4.1. Numerically Generated Surface to Additive Manufactured

Initially, a study was carried out to quantify the difference between the generated rough surface topographies and the 3D-printed masters for the subsequent replication studies. This was required to assess the inevitable difference between the computer-generated topography and the 3D-printed rough surface used for replication. The difference will vary depending on the printer being used. This difference must be quantified so that the variability can be accounted for when designing a rough surface topography if a specific roughness or complex topography is desired. For our work, three distinct topographies were used for investigation (Sq: 25, 50, and 100 μm). These were not required to replicate the designed topographies exactly as we were aware there would be some variability introduced at the additive manufacture stage.

Figure 5 shows the measured Sq values gathered from stitched optical scans of the full 3D-printed topographies (**Table 1** shows the data). The stitched scans allow for a complete analysis of the printed topographies. The data indicates that the 3D-printed surfaces have slightly lower roughness compared to the target (numerically generated) roughness. The results also indicate that the difference in roughness between the design and 3D-printed surface increases with roughness. This difference is partly introduced by the limiting resolution of the printer. However, it is hypothesized that the print difference is largely influenced by the increased slope of the topography with the rougher topographies. The steeper slope at higher roughness values means that the asperities making up the topography are essentially high aspect ratio microstructures. It is very difficult to 3D print high-aspect microstructures.[58–60] **Table 2** details the slope associated with the respective rough surfaces at crucial points in the fabrication process. While it is possible to achieve high-aspect-ratio structures on a microscale via 3D printing, it is typically a difficult process that requires rigorous optimization for the specific topography, material used, and device. Therefore, while it would be possible to increase the topography dataset to 3D print translation quality, this would require more versatile 3D printing techniques/equipment than were available. If higher roughness topographies are required, then the design to 3D print percentage difference should be considered accordingly. With some experience, it should be possible to compensate in the design surface for the change introduced during printing and produce the required master surface.
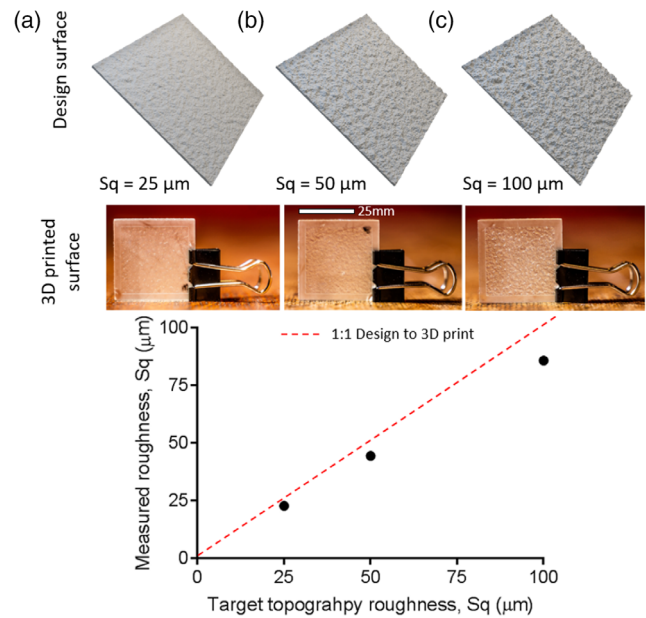

Figure 5. Plot indicating the difference between the measured roughness, Sq, of the 3D-printed samples and the computer-generated (target) rough surface datasets. Inset photographs included show the three 3D-printed topographies: a) 25 μm, b) 50 μm, and c) 100 μm. Each measured result is the average from five similar samples.

Table 1. Measured roughness of the 3D-printed topographies (compared to the numerically generated "design roughness").

Design roughness, Sq [μm]	3D-printed roughness, Sq [μm]	S.D. [μm]	% Difference
25	22.72	0.21	9.1
50	44.35	0.43	11.3
100	85.68	0.57	14.3

4.2. Rough Surface Replication Study

As discussed earlier, two approaches were used to assess the replication quality of the injection molded and polymer cast surfaces: cross-correlation and a mean surface difference approach. **Figure 6** shows the results for the cross-correlation analysis, while **Figure 7** indicates the equivalent plot for the difference measurement method. Data is shown for the three roughness levels comparing the injection molded polystyrene with the three replicas produced by polymer casting: epoxy, PDMS, and PVS ultra-low viscosity. Generally, the replication of the 25 μm surface was very good with CCR ranging from 0.74 for the injection molding to 0.82 for the ultra-low viscosity PVS. The casting method had very similar replication results across the polymer materials for the 25 μm surface. High CCR values for this topography indicate the high quality of replication. These results are supported by the corresponding low values from the difference measurement approach for the 25 μm case in Figure 7 (i.e., indicating low levels of the mean difference between the two surfaces).

Table 2. Measured slope, Sdq, of the numerical designs, 3D-printed surfaces, and polymer replica surfaces.

Roughness instance	RMS surface slope, Sdq [µm]		
RMS surface height, Sq [µm]	Design	3D print	Replica
25	0.071	0.41 ± 0.02	PDMS 0.34 ± 0.01
			PVS 0.34 ± 0.02
			Epoxy 0.46 ± 0.01
			Polystyrene 0.49 ± 0.04
50	0.141	0.59 ± 0.03	PDMS 0.62 ± 0.02
			PVS 0.65 ± 0.03
			Epoxy 0.75 ± 0.04
			Polystyrene 0.76 ± 0.03
100	0.282	0.88 ± 0.01	PDMS 1.2 ± 0.08
			PVS 1.02 ± 0.06
			Epoxy 1.11 ± 0.08
			Polystyrene 1.11 ± 0.02

As the roughness of the dataset increased, the replication quality generally dropped. This is seen in both the CCR and difference measurement data. It is hypothesized that this is largely due to the increase in slope associated with magnifying the roughness of this surface. This likely results in a decrease in the polymers' ability to correctly fill the micro- and nano-features of the 3D-printed designs. This behavior has also been evident in previous studies of biomimetic polymer replication[15,42,43] where the increasing complexity of the leaf topographies resulted in poorer polymer replication. There is good similarity exhibited by the replicas of the 50 µm topography across all methods, with only slightly reduced replication in comparison to the 25 µm surface. High replication at 50 µm is demonstrated across all replication methods, as indicated by the high CCR values and low levels of mean difference. A significant drop in replication quality is evident for the injection molding method for the 100 µm topography as evident from the lower CCR value of 0.46 and the higher mean difference. For the casting method, there is

a drop in replication quality for the PDMS and PVS at 100 µm, but not as significant as seen for the injection molding method. Table 2 confirms that the surface slopes for the 3D-printed master surfaces do indeed increase with surface roughness. For instance, for the 3D-printed masters, the root mean square surface slope (Sdq) increases from 0.41 to 0.88 as the roughness goes from 25 to 100 µm. This is also reflected in the polymer replicas, where we see a similar trend. The measured slopes indicate that decreasing replication quality appears to follow from increased surface slopes. The ultra-low viscosity epoxy shows the most consistent results across the three roughness levels. This is consistent across all 3D-printed surfaces and polymer replicas. However, these results also indicate that polymers with extremely low viscosities can facilitate high-quality replication using the casting method even when replicating relatively complex rough surface topographies. The low viscosity will inevitably allow the polymer to capture the micro and nano-scale features with greater accuracy due to increased filling capability —we study this important effect of viscosity in more detail in Section 4.5.

The injection molding results were disappointing for the 100 µm surface and this is somewhat surprising as the same equipment has previously been used in a previous study to replicate challenging nano-structured topographies in Stormonth-Darling et al.[20] The working hypothesis is that the injection molding parameters require further optimization for the replication of the high Sq rough surfaces used in the present study. There are a significant number of variables that can influence the replication quality of the molding cycle including injection velocity, holding time and pressure, tooling temperature, etc.[20,32,33,36] These all have individual influence over the quality of replication; therefore, it would seem reasonable that the parameters will not have been optimally tuned to facilitate the best replication possible for these rough surface topographies. Non-optimum molding parameters can lead to incomplete filling of the mold and poor replication. Another source of error could be that the polymer may not have cooled fully before being ejected, resulting in a distortion of the replicated surface of the sample as it exits the mold cavity and separates from the inlay. It is recommended that a full optimization of the molding parameters for injection molding be
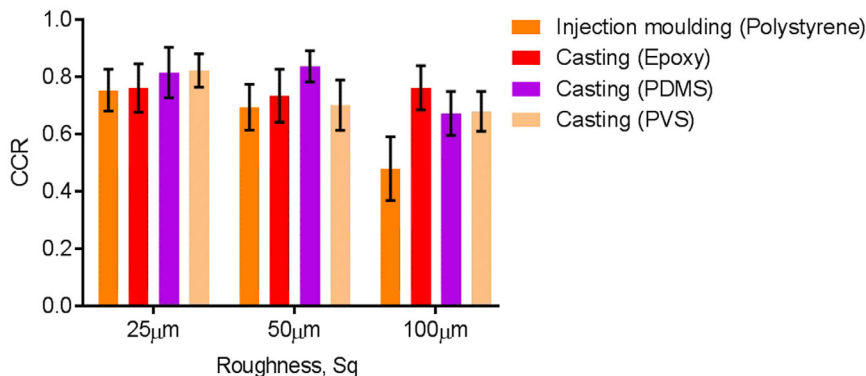

Figure 6. Cross-correlation ratio between replica surfaces and 3D-printed master for design roughness levels (Sq) of 25, 50, and 100 µm. Results are shown comparing the injection molded (polystyrene) result to the three polymer cast replicas (ultra-low viscosity epoxy, polydimethylsiloxane (PDMS), and ultra-low viscosity PVS). Each result is the mean from 12 similar samples.
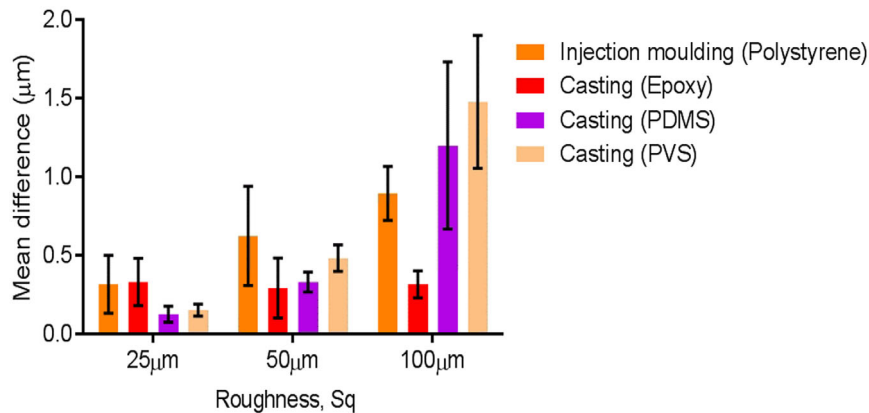
Figure 7. Mean surface difference between replica surfaces and 3D-printed master for design roughness levels (Sq) of 25, 50, and 100 μm. Results are shown comparing the injection molded (polystyrene) result to the three polymer cast replicas (ultra-low viscosity epoxy, PDMS, and ultra-low viscosity polyvinyl siloxane (PVS)). Each result is the mean from 12 similar samples.

carried out to improve the replication capabilities, especially when molding more complex rough surface topographies. Clearly, further optimisation is likely to improve replication quality for injection molding. Full numerical results are available in **Table 3**.

4.3. Injection Molding Inlay Durability

Typically, it is desirable to have an injection molding inlay with high durability. This allows the inlay to withstand the harsh environment during the molding cycle and enables more mold runs using the same inlay while preserving part quality. Conventionally, the way to assess inlay durability, is to take components at set points during the mold run and compare the quality of the parts. For example, parts from different stages of evolution of a single molding cycle (i.e., different shot numbers) can be compared to ensure the inlay has not undergone any significant degradation preventing high-quality manufacture during the run. The process developed here is aimed at rapid prototyping surfaces for study in a research environment; hence, the molding runs were kept relatively short varying from 30 to 50 components per run. Typically, industrial production runs would be far longer, reaching hundreds of components. Convery et al.[33] confirmed that an inlay of the same 3D-printed material will not suffer significant degradation even after 500

parts are fabricated using the inlay for an injection molding run. They found that the micro-channels in their designs were still within acceptable error margins even after 500 parts were produced.

The durability study here considered Parts 10, 20, and 30 to confirm that there was no significant degradation of the respective rough surfaces on the molding inlay. **Figure 8** shows the result of the study. Figure 8a indicates the cross-correlation values at different shot numbers while Figure 8b gives the equivalent mean difference results (compared with the 3D-printed master). Overall, the data in Figure 8 is quite consistent across the shot numbers for each of the quality measurement techniques. This indicates that the replicas generated at set points in the injection molding runs have satisfactorily equivalent topographies. Here we have shown that there is no significant degradation to Part 30. This is extremely important if the injection molding process is to be used to produce identical components in a research or applied environment. It remains for further study to examine if the rough surface inlay can withstand production up to the level of hundreds of parts. However, this study indicates that the rough surface 3D-printed inlays produced here can be used to produce a significant number of extremely similar samples in a short space of time which should be sufficient to provide for several applications. Full numerical results for the inlay study are given in **Table 4**.

Table 3. Cross-Correlation ratio (CCR) and mean surface difference (μm) between replica surfaces and 3D-printed master for design roughness levels (Sq) of 25, 50, and 100 μm. Results are shown comparing the injection molded (polystyrene) result to the three polymer cast replicas (ultra-low viscosity epoxy, ultra-low viscosity PVS, and PDMS). Each result is the mean from 12 similar samples.

	Cross-correlation ratio [CCR]			Mean Difference Measurement [μm]		
	Sq 25 μm	Sq 50 μm	Sq 100 μm	Sq 25 μm	Sq 50 μm	Sq 100 μm
Injection Molding (Polystyrene)	0.74 ± 0.07	0.69 ± 0.09	0.46 ± 0.14	0.32 ± 0.27	0.67 ± 0.43	0.91 ± 0.09
Casting (Epoxy, ultra-low viscosity)	0.76 ± 0.09	0.74 ± 0.09	0.76 ± 0.08	0.33 ± 0.15	0.3 ± 0.19	0.32 ± 0.09
Casting (PVS, ultra-low viscosity)	0.82 ± 0.06	0.70 ± 0.09	0.68 ± 0.07	0.15 ± 0.04	0.48 ± 0.08	1.48 ± 0.42
Casting (PDMS)	0.82 ± 0.9	0.84 ± 0.06	0.67 ± 0.08	0.13 ± 0.05	0.33 ± 0.06	1.2 ± 0.53

**ADVANCED
SCIENCE NEWS**

www.advancedsciencenews.com

**ADVANCED
ENGINEERING
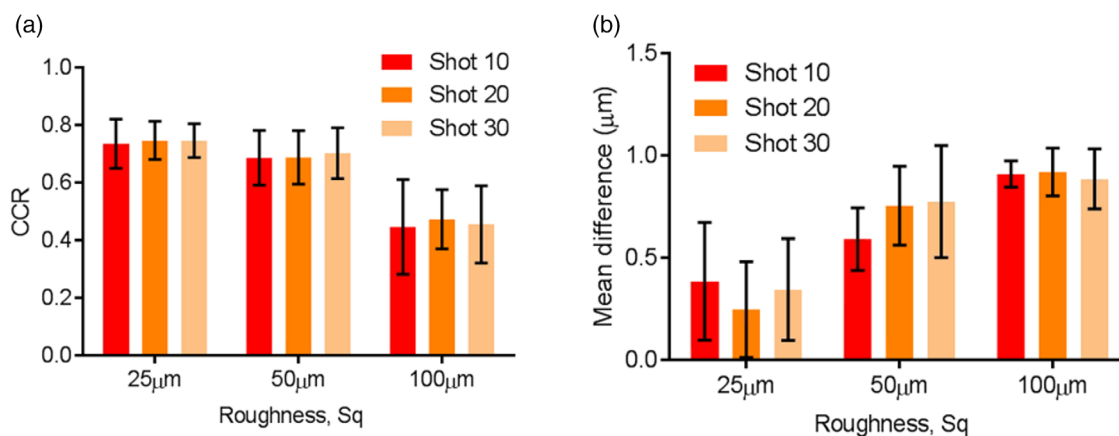MATERIALS**

www.aem-journal.com

(a)

(b)

Figure 8. Injection molding inlay durability study: a) cross-correlation ratio (CCR) between injection molded (PS) replica surfaces and 3D-printed master for mold shots 10, 20, and 30 and b) mean difference measurement between injection molded (PS) replica surfaces and 3D-printed master for mold shots 10, 20, and 30 The consistency across the shot numbers highlights good inlay durability and repeatability of the injection molding process. Results shown for each roughness level.

Table 4. Injection molding inlay durability data indicating results for cross-correlation ratio (CCR) and mean difference between injection molded (PS) replica surfaces and 3D-printed master for mold shots 10, 20, and 30. The consistency across the shot numbers highlights good inlay durability.

	CCR			Difference Measurement [µm]		
	Sq 25 µm	Sq 50 µm	Sq 100 µm	Sq 25 µm	Sq 50 µm	Sq 100 µm
Shot 10	0.74 ± 0.09	0.69 ± 0.09	0.45 ± 0.16	0.39 ± 0.29	0.59 ± 0.36	0.91 ± 0.06
Shot 20	0.75 ± 0.07	0.69 ± 0.09	0.47 ± 0.1	0.25 ± 0.23	0.75 ± 0.48	0.92 ± 0.12
Shot 30	0.74 ± 0.06	0.7 ± 0.09	0.46 ± 0.13	0.34 ± 0.25	0.77 ± 0.37	0.89 ± 0.15

4.4. Rough Surface Tailoring

The generated surfaces used in our research were typically kept to consistent PSD parameters with only the areal Sq roughness being varied for the subsequent fabrication studies. However, if required the PSD parameters used to generate the surfaces can be altered to produce tailored surfaces with tuned topographies to suit the research requirement. This is a rather powerful aspect of the surface generation code developed in Section 2.1. To illustrate the tailoring capability, an attempt was made to generate and print surfaces having different frequency/wavelength characteristics. The purpose of the study is to determine how well the 3D-printed surfaces can reproduce predefined changes in frequency/wavelength. The PSD is defined by an upper and lower frequency (f_l and f_s). These frequencies influence the waveform range that the asperities of the surface can fit.[53] Altering these frequencies modifies the shape of the generated topography. Four distinct topographies with varied upper and lower frequency bounds were generated. **Figure 9** shows the four designed/generated topographies (top) together with the resulting 3D print efforts (bottom). These surfaces were designed to go from low frequency, long wavelength (Figure 9a) to high frequency, short wavelength (Figure 9d) while keeping the Sq roughness and Hurst number constant. The frequency range also increases from Figure 9a–d. A summary of the parameters used to generate the four surfaces is given in **Table 5**.

Looking at Figure 9, we can clearly see that the topographies are quite different in nature even though their amplitude-based

roughness values (e.g., Sq) are equivalent (i.e., Figure 9a showing longer wavelengths and widely dispersed asperities and Figure 9d showing short wavelength frequent asperities). Comparing the 3D-printed scans (bottom images in Figure 9) with the generated surfaces (top images in Figure 9), we see that 3D printing has largely been able to capture the changes in frequency characteristics. Indeed this is confirmed quantitatively if we look at the surface gradient and autocorrelation values for the 3D-printed surfaces in Table 5. Consistent with the move to higher frequencies, the surface gradient Sdq increases and the autocorrelation length Sal (an indicator of characteristic wavelength) decreases. This is in line with the prescribed frequency increase, since higher frequencies (with the same roughness), necessarily require steeper gradients and shorter wavelengths. We also see that the Sq of the 3D-printed surfaces remains roughly constant (as prescribed for the generated surfaces). This study indicates the ease with which 3D-printed rough surface topographies can be tailored for specific research applications. Certain desirable characteristics can be kept consistent, while key parameters can be varied for investigation. Highlighting the fabrication tool's versatility and transferable nature.

4.5. Effect of Viscosity in Rough Surface Casting

In this section, we examine the effect of viscosity in more detail and look at how varying the viscosity of a polymer resin affects the replication quality of the rough surfaces produced. The proprietary PVS resins (President, Coltene Whaledent, Altstätten,
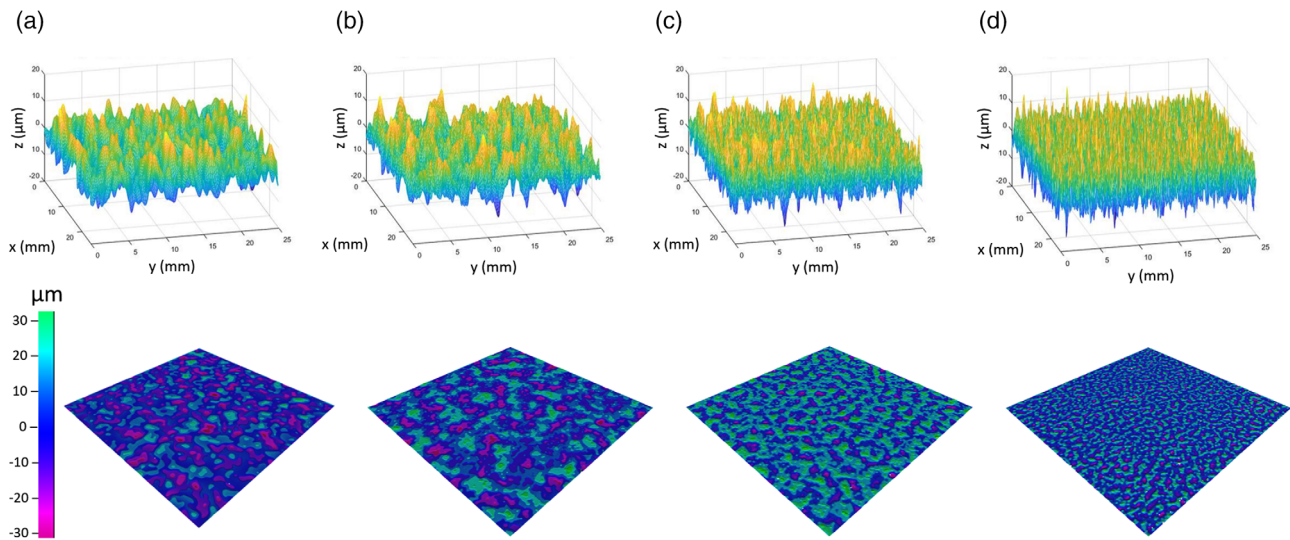
Figure 9. Surface tailoring results indicating the ability to fabricate surfaces with varying frequency characteristics. Figure shows the generated topographies (top) and the as-produced 3D-printed surfaces (bottom). The frequency cut-off bands are varied from left to right with upper and lower frequency cut-offs (and frequency range) increasing from left to right according to [f_l, f_s] (Units of 1/mm): a) [5, 32], b) [5, 64], c) [10, 128], and d) [20, 256]. Essentially, (a) is low frequency, long wavelength and (d) is high frequency, short wavelength. The 3D-printed surfaces reproduce the changes extremely well. The Sq and Hurst number H are maintained constant.

Table 5. Parameters and results associated with the rough surface tailoring study. The table shows key surface parameters of the generated surfaces and the corresponding 3D-printed surfaces for four different design surface frequency ranges denoted by a), b), c), and d) corresponding to Figure 9. Hurst number, H = 0.7 for each case.

Surface instance based on frequency bounds	Lower cut-off frequency, f_l [1/mm]	Upper cut-off frequency, [f_s] [1/mm]	Generated roughness, Sq [µm]	3D-printed roughness, Sq [µm]	3D-printed gradient, Sdq	3D-printed autocorrelation length, Sal [µm]
(a)	5	32	25	23.38	0.27	755.2
(b)	5	64	25	23.36	0.29	780.7
(c)	10	128	25	22.49	0.35	490.3
(d)	20	256	25	22.97	0.37	253.9

Switzerland) were selected for the study—see Section 2.3.3. The company produces four types of very similar PVS resins, but have varying degrees of viscosity making them an ideal selection for a viscosity study. The four resin types produced are designated as: ultra-low viscosity, low viscosity, standard viscosity, and high viscosity. Viscosity measurements were performed with a modular compact rheometer (MCR 302, Anton Paar, Austria) equipped with either of the following two geometries: parallel plates of 50 mm diameter or cone & plate of 50 mm diameter and 1° angle. The curing process of the materials was monitored by measuring the time behavior of their viscoelastic moduli. All the measurements were performed by keeping the following three experimental parameters constant: a temperature of 22 °C, a strain amplitude of 20%, and a frequency of 20 Hz (for three repeat batches on each resin type). For the viscosity study, a single roughness level of $Sq = 25$ µm was used. The modified PVS casting method (detailed in Section 2.3.3) was used for each resin and repeated three times per resin to allow for three replica surfaces from each resin type. Optical scans of the surfaces were then taken using the Bruker–Alicona 3D

InitinteFocus profilometer and the replication quality was again assessed by calculating the CCR and mean difference measurement with respect to the 3D-printed master. **Figure 10** shows the
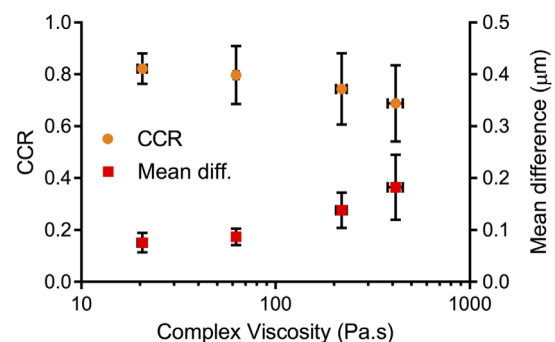

Figure 10. Study on the effect of viscosity (of PVS resin) in the casting process: CCR and mean difference measurement (against 3D-printed master) versus complex viscosity. Each result is the mean from 3 surface replicas. 25 µm design used for analysis and replication.

**ADVANCED
SCIENCE NEWS**

www.advancedsciencenews.com

**ADVANCED
ENGINEERING
MATERIALS**

www.aem-journal.com

Table 6. Effect of resin viscosity on the quality of casting replication of PVS from the 3D-printed master assessed via cross-correlation ratio and mean difference measurement. 25 µm design used for analysis and replication.

	Complex viscosity [Pa s]	Cross-correlation ratio [CCR]	Mean difference measurement [µm]
PVS (ultra-low viscosity)	20.60 ± 1.12	0.82 ± 0.06	0.15 ± 0.04
PVS (low viscosity)	62.64 ± 1.68	0.79 ± 0.11	0.17 ± 0.03
PVS (standard viscosity)	218.6 ± 13.67	0.74 ± 0.14	0.28 ± 0.07
PVS (high viscosity)	414.7 ± 36.93	0.36 ± 0.13	0.36 ± 0.13

result of the study where CCR and mean difference are plotted against complex viscosity. Each result is the mean from three surface replicas. CCR decreases with viscosity while the mean difference increases correspondingly. This clearly indicates that the replication quality gradually reduces for higher viscosities. The CCR measurement drops from 0.82 with the ultra-low viscosity resin to 0.69 for the high viscosity resin. The numerical data is summarized in **Table 6** for reference. The results suggest that the more viscous resins have a reduced flowability and ability to fully fill in the valleys and troughs in the rough surface topographies. It is, therefore, reasonable to conclude that low viscosity polymer resins should be used where possible when high-quality replicas of rough surface topographies are required.

4.6. Applications for Advanced Tailoring of Rough Surfaces

We have demonstrated the controlled production of advanced 3D-printed rough surface topographies and their rapid replication via casting and injection molding. The method is tuneable allowing for the production of surface topographies displaying user-defined characteristics. The ease of operation, short throughput time, range of available (polymer) materials, and high-quality replication emphasize the transferable and versatile nature of the technique. So, what are the applications of being able to produce these advanced rough surface topographies? It turns out that there are several applications and this is because very many interfacial and surface processes and phenomenon are sensitive to surface roughness. The most obvious applications are in experimental research, where having precise control over surface parameters allows us to determine their effect on these phenomena. There are also situations where we might want to retain a near identical rough surface in several tests. We take a look at some of these phenomena next.

In tribology, phenomena like friction,[61] adhesion,[62] contact stiffness,[63] lubrication[64,65] and sealing effectiveness[66] are all sensitive to roughness. Example applied studies include surface replication of biological topographies to see how certain microstructures influence adhesion mechanisms,[67] and investigation of rubber friction using 3D-printed randomly rough surfaces.[68] The ability to control and repeat rough surface topographies is likely to be useful in a wide range of tribological tests exploring these phenomena. In the mechanics of materials, failure and fracture behavior are also affected by surface roughness.[69] In fluid dynamics, surface roughness influences the generation of turbulent boundary layers and affects important factors like aerodynamic drag.[70] In the biosphere, roughness can affect biological growth on rough surfaces. Khoshkhoo et al.[71] looked at the role played by roughness in algae growth for example. The team reverse engineered rough surface topographies of rocks for the 3D printing of test surfaces. This allowed them to examine how different rough surfaces affect algae growth. Similar studies have explored the concept of algae growth on 3D-printed rough surfaces and components used in water treatment.[72–74] All these works could potentially benefit from the methods employed in our research as they would allow more advanced control over surface characteristics as well as offer a wider selection of material options. The haptic and tactile response has even been explored with reference to rough surfaces. Sahli et al.[75] 3D-printed a range of large rough surface polymer pads with varied microstructures and surface parameters. They then had participants physically interact with the rough surfaces to study tactile perception and determine if participants could distinguish between the surfaces. Haptic and tactile response is another area of research where our approach could be utilized. As a final example of the breadth of possible applications, we cite the ongoing triboelectric nanogenerator research where electrical output has already been shown to be sensitive to the surface roughness of the contacting surfaces.[76–78] Here, in fact, the present authors are already using the approach developed here in ongoing triboelectric research. Hence, there would appear to be quite a breadth of possible applications for the approach in experimental research across various fields of engineering. As we have seen, some groups have already 3D-printed basic rough surfaces in their studies, but the key addition in our work is the powerful advanced numerical surface generation tool and the two versatile rapid replication routes that open up advantages in terms of high throughput and a wider selection of materials and surface properties.

5. Conclusions

In this work, we have developed different approaches for the rapid fabrication of advanced predesigned rough surface topographies in various polymers. Rough surfaces with predefined topography characteristics were first generated numerically. These were then 3D-printed to produce a master surface which was used to produce replicas via two alternative routes: injection molding and casting. Injection molded surfaces were produced in polystyrene and polymer cast surfaces were fabricated in epoxy, PDMS, and PVS. Three different roughness levels were produced at $Sq = 25$, 50, and 100 µm and a separate study was carried out with varying frequency content for the 25 µm case. Results showed excellent reproduction of the numerical surface by 3D printing and excellent replication of the 3D-printed master surface in the final replicas. At the 25 µm roughness level, replication quality (assessed via the cross-correlation ratio - CCR) was high reaching 0.82 for the casting of low viscosity PVS and PDMS and up to 0.74 for injected molded polystyrene. Reproduction quality is clearly slightly higher for the polymer cast samples, but throughput will be lower than for injection molding. Reproduction quality decreased somewhat with increasing roughness (especially for injection molding) likely due to the increased slopes and aspect ratios of the surface

features. The casting of low viscosity epoxy defied this trend yielding the most consistent results across the three roughness levels (CCR = 0.76 at both 25 and 100 μm roughness). Results also demonstrated the ability of the 3D-printed surface to replicate adjustments in the amplitude and frequency content of the surfaces; thus, demonstrating the usefulness of the method for tailoring of surface roughness. The key novelties of the work are the ability to generate advanced user-defined rough surface topographies and the capability to rapidly replicate the surfaces effectively in the wider range of polymers as enabled by the casting and injection molding steps. For injection molding, we also demonstrated good mold durability over some 30 repeats. For polymer casting, we showed that replication quality reduces with resin viscosity meaning that low viscosity polymers are advisable as they allow penetration of the resin into the more challenging surface valleys.

This ability to rapidly produce rough surface topographies in a versatile range of polymer materials according to a flexible surface generation approach is likely to be a powerful tool. Surface roughness is ubiquitous in both natural and engineered surfaces alike. The main applications are thought to be in experimental research environments involving interfacial or surface processes sensitive to roughness. There are several examples ranging from friction, adhesion, and lubrication in tribology to aerodynamic drag caused by rough surfaces in fluid dynamics applications to the biological examples of algae growth or cell growth on rough surfaces. This work will prompt more advanced experimental studies on how surface topography characteristics affect phenomena such as those mentioned earlier.

Supporting Information

Supporting Information is available from the Wiley Online Library or from the author.

Conflict of Interest

The authors declare no conflict of interest.

Data Availability Statement

The data that support the findings of this study are available from the corresponding author upon reasonable request.

[1] A. Hamilton, J. Perris, N. Convery, D. M. Mulvihill, N. Gadegaard, *Macromol. Mater. Eng.* **2021**, *306*, 2100223.

[2] R. M. Amin, S. Knowlton, A. Hart, B. Yenilmez, F. Ghaderinezhad, S. Katebifar, M. Messina, A. Khademhosseini, S. Tasoglu, *Biofabrication* **2016**, *8.*, 022001.

[3] S. Kumar, P. Bhushan, M. Pandey, *J. Micromanufact.* **2019**, *2*, 175.

[4] Z. Wang, Z. Yi, M. Qin, Q.-A. Huang, *IEEE Trans. Instrum. Measur.* **2021**, *70*, 19507408.

[5] S. Juodkazis, Y. Nishi, H. Misawa, V. Mizeikis, O. Schecker, R. Waitz, P. Leiderer, E. Scheer, *Opt. Exp.* **2009**, *17*, 15308.

[6] P. Gečys, G. Račiukaitis, M. Gedvilas, A. Selskis, *Eur. Phys. J. Appl. Phys.* **2009**, *46*, 12508.

[7] P. Engelhart, N. P. Harder, R. Grischke, A. Merkle, R. Meyer, R. Brendel, *Progr. Photovolt. Res. Appl.* **2007**, *15*, 237.

[8] E. Rodríguez-Vidal, C. Sanz, C. Soriano, J. Leunda, G. Verhaeghe, *J. Mater. Process. Technol.* **2016**, *229*, 668.

[9] A. Kurella, N. B. Dahotre, *J. Biomater. Appl.* **2005**, *20*, 5.

[10] A. Y. Vorobyev, C. Guo, *Appl. Surf. Sci.* **2007**, *253*, 7272.

[11] K. Koch, A. J. Schulte, A. Fischer, S. N. Gorb, W. Barthlott, *Bioinspir. Biomimet.* **2008**, *3*, 046002.

[12] A. J. Schulte, K. Koch, M. Spaeth, W. Barthlott, *Acta Biomater.* **2009**, *5*, 1848.

[13] W. Wu, R. M. Guijt, Y. E. Silina, M. Koch, A. Manz, *RSC Adv.* **2016**, *6*, 22469.

[14] L. Gitlin, P. Schulze, D. Belder, *Lab Chip* **2009**, *9*, 3000.

[15] B. Prüm, H. F. Bohn, R. Seidel, S. Rubach, T. Speck, *Acta Biomater.* **2013**, *9*, 6360.

[16] S. Bin Jaber, A. Hamilton, Y. Xu, M. E. Kartal, N. Gadegaard, D. M. Mulvihill, *Tribol. Int.* **2021**, *153*, 106563.

[17] J. Perris, Y. Xu, M. E. Kartal, N. Gadegaard, D. M. Mulvihill, *Tribology Letters* **2021**, Vol *69*, 106,.

[18] K. Willis, E. Brockmeyer, S. Hudson, I. Poupyrev, in *Proc. of the 25th Annual ACM Symp. on User Interface Software and Technology*, **2012**, pp. 589–598.

[19] S. Waheed, J. M. Cabot, N. P. Macdonald, T. Lewis, R. M. Guijt, B. Paull, M. C. Breadmore, *Lab Chip* **2016**, *16*, 1993.

[20] J. M. Stormonth-Darling, N. Gadegaard, *Macromol. Mater. Eng.* **2012**, *297*, 1075.

[21] T. Hofstätter, M. Mischkot, D. B. Pedersen, G. Tosello, H. N. Hansen, in *Proc. of ASPE Summer Topical Meeting 2016: Dimensional Accuracy and Surface Finish in Additive Manufacturing*, **2016**.

[22] Y. Zhang, D. B. Pedersen, A. S. Gøtje, M. Mischkot, G. Tosello, *J. Manuf. Process.* **2017**, *27*, 138.

[23] K. Koch, B. Bhushan, W. Barthlott, *Prog. Mater Sci.* **2009**, *54*, 137.

[24] B. Zhang, H. Lee, D. Byun, *Adv. Eng. Mater.* **2020**, *22*, 1901362.

[25] S. Bose, S. Vahabzadeh, A. Bandyopadhyay, *Mater. Today* **2013**, *16*, 496.

[26] W. Zhu, X. Ma, M. Gou, D. Mei, K. Zhang, S. Chen, *Curr. Opin. Biotechnol.* **2016**, *40*, 103.

[27] A. V. Do, B. Khorsand, S. M. Geary, A. K. Salem, *Adv. Healthcare Mater.* **2015**, *4*, 1742.

[28] U. Jammalamadaka, K. Tappa, *J. Funct. Biomater.* **2018**, *9*, 22.

[29] A. I. Bennett, K. L. Harris, K. Schulze, J. M. Urueña, A. J. McGhee, A. A. Pitenis, M. H. Müser, T. E. Angelini, W. G. Sawyer, *Tribol. Lett.* **2017**, *65*, 1.

[30] M. H. Müser, et al., *Tribol. Lett.* **2017**, 65.

[31] U. M. Attia, S. Marson, J. R. Alcock, *Microfluid. Nanofluid.* **2009**, 7, 1.

[32] W. Michaeli, A. Spennemann, R. Gärtner, *Microsyst. Technol.* **2002**, 8, 55.

[33] N. Convery, I. Samardzhieva, J. M. Stormonth-Darling, S. Harrison, G. J. Sullivan, N. Gadegaard, *Macromol. Mater. Eng.* **2021**, 306, 2100464.

[34] J. Greener, R. Wimberger-Friedl, in *Precision Injection Molding*, Carl Hanser, Munich **2006**.

[35] B. Sha, S. Dimov, C. Griffiths, M. S. Packianather, *J. Mater. Process. Technol.* **2007**, 183, 284.

[36] J. M. Stormonth-Darling, R. H. Pedersen, C. How, N. Gadegaard, *J. Micromech. Microeng.* **2014**, 24, 075019.

[37] H. N. Hansen, R. J. Hocken, G. Tosello, *CIRP Ann.* **2011**, 60, 695.

[38] J. Giboz, T. Copponnex, P. Mélé, *J. Micromech. Microeng.* **2007**, 17, R96.

[39] N. Zhang, A. Srivastava, B. Kirwan, R. Byrne, F. Fang, D. J. Browne, M. D. Gilchrist, *J. Micromech. Microeng.* **2015**, 25, 095005.

[40] N. Zhang, A. P. Srivastava, D. J. Browne, M. D. Gilchrist, *J. Mater. Process. Technol.* **2016**, 231, 288.

[41] M. Mischkot, H. N. Hansen, D. B. Pedersen, in *15th Int. Conf. of the European Society for Precision Engineering and Nanotechnology* **2015**.

[42] C. Kumar, V. Le Houérou, T. Speck, H. F. Bohn, *Roy. Soc. Open Sci.* **2018**, 5, 172132.

[43] C. Kumar, A. Palacios, V. A. Surapaneni, G. Bold, M. Thielen, E. Licht, T. E. Higham, T. Speck, V. Le Houérou, *Philos. Trans. Roy. Soc. A.* **2019**, 377, 20180265.

[44] M. Sun, C. Luo, L. Xu, H. Ji, Q. Ouyang, D. Yu, Y. Chen, *Langmuir* **2005**, 21, 8978.

[45] M. Salta, J. A. Wharton, P. Stoodley, S. P. Dennington, L. R. Goodes, S. Werwinski, U. Mart, R. J. Wood, K. R. Stokes, *Philos. Trans. Roy. Soc. A: Math. Phys. Eng. Sci.* **2010**, 368, 4729.

[46] H. Yan, Q. Wu, C. Yu, T. Zhao, M. Liu, *Adv. Mater. Interfaces* **2020**, 7, 2000966.

[47] Z. Huang, S. Yang, H. Zhang, M. Zhang, W. Cao, *Sci. Rep.* **2015**, 5, 1.

[48] B. McDonald, P. Patel, B. Zhao, *Chem. Eng. Process Tech.* **1988**, 1, 1012.

[49] S. M. Lee, T. H. Kwon, *Nanotechnology* **2006**, 17, 3189.

[50] P. Kim, K. W. Kwon, M. C. Park, S. H. Lee, S. M. Kim, K. Y. Suh, *Biochip J.* **2008**, 2, 1.

[51] Y. Z. Hu, K. Tonder, *Int. J. Mach. Tools Manuf.* **1992**, 32, 83.

[52] J. J. Wu, *Tribol. Int.* **2000**, 33, 47.

[53] V. A. Yastrebov, G. Anciaux, J.-F. Molinari, *Int. J. Solids Struct.* **2015**, 52, 83.

[54] Y. Xu, R. L. Jackson, *Tribol. Int.* **2017**, 105, 274.

[55] Formlabs, *Clear Resin SDS*, ASME, New York **2016**.

[56] J. Song, T. Vorburger, in *Third Int. Symp. Precision Mechanical Measurements*, Inter. Society for Optics and Photonics, Washington pp. 62801T 1–8.

[57] Alicona Help User's Manual, IF MeasurementSuite 5.1. Bruker Alicona, Austria, **2013**.

[58] A. Kain, C. Mueller, H. Reinecke, *Proc. Chem.* **2009**, 1, 750.

[59] K. J. Krieger, N. Bertollo, M. Dangol, J. T. Sheridan, M. M. Lowery, E. D. O'Cearbhaill, *Microsyst. Nanoeng.* **2019**, 5, 1.

[60] B. G. Compton, J. A. Lewis, *Adv. Mater.* **2014**, 26, 5930.

[61] E. Rabinowicz, *Friction and Wear of Materials*, 2nd ed., Wiley-Interscience, Hoboken, NJ **1995**.

[62] K. N. G. Fuller, D. Tabor, *Proc. Roy. Soc. A: Math. Phys. Eng. Sci.* **1975**, 345.

[63] C. Campaña, B. J. N., Persson, Müser, *J. Phys. Condens. Matter* **2011**, 23.

[64] R. Larsson, *Wear* **2009**, 42, 512.

[65] A. G. Shvarts, V. A. Yastrebov, *J. Mech. Phys. Solids* **2018**, 119, 140.

[66] B. N. J. Persson, O. Albohr, U. Tartaglino, A. I. Volokitin, E. Tosatti, *J. Phys. Condens. Matter* **2005**, 17.

[67] C. Kumar, D. Favier, T. Speck, V. Le Houérou, *Adv. Mater. Interfaces* **2020**, 7, 2000969.

[68] M. M. Kanafi, A. J. Tuononen, L. Dorogin, B. N. Persson, *Wear* **2017**, 376, 1200.

[69] S. Sneddon, Y. Xu, M. Dixon, D. Rugg, P. Li, D. M. Mulvihill, *Mater. Des.* **2021**, 200.

[70] A. Busse, T. O. Jelly, *Flow Turbul. Combust.* **2020**, 104, 331.

[71] A. Khoshkhoo, A. L. Carrano, D. M. Blersch, K. Kardel, *Plos One* **2019**, 14, 0219150.

[72] A. L. Carrano, D. M. Blersch, K. Kardel, A. Khoshkhoo, presented at *5th Int. Conf. on Surface Metrology*, April 2016, Poznan, Poland.

[73] K. Kardel, A. L. Carrano, D. M. Blersch, M. Kaur, *3D Print. Addit. Manufact.* **2015**, 2, 12.

[74] O. Elliott, S. Gray, M. McClay, B. Nassief, A. Nunnelley, E. Vogt, J. Ekong, K. Kardel, A. Khoshkhoo, G. Proaño, D. M. Blersch, *J. Contemp. Water Res. Educ.* **2017**, 160, 144.

[75] R. Sahli, A. Prot, A. Wang, M. H. Müser, M. Piovarči, P. Didyk, R. Bennewitz, *Sci. Rep.* **2020**, 10, 1.

[76] A. G. Shvarts, Y. Xu, G. Min, I. Athanasiadis, L. Kaczmarczyk, D. M. Mulvihill, C. J. Pearce, in *Proc. of the UKACM 2021 Conf.*, Loughborough, UK **2021**.

[77] Y. Xu, G. Min, N. Gadegaard, R. Dahiya, D. M. Mulvihill, *Nano Energy* **2020**, 76, 105067.

[78] G. Min, Y. Xu, P. Cochran, N. Gadegaard, D. M. Mulvihill, R. Dahiya, *Nano Energy* **2021**, 83, 105829.